Journal of Building Performance Simulation

ISSN: 1940-1493 (Print) 1940-1507 (Online) Journal homepage: http://www.tandfonline.com/loi/tbps20

Experimental and numerical study of airflow distribution in an aircraft cabin mock-up with a gasper on

Ruoyu You, Jun Chen, Zhu Shi, Wei Liu, Chao-Hsin Lin, Daniel Wei & Qingyan Chen

To cite this article: Ruoyu You, Jun Chen, Zhu Shi, Wei Liu, Chao-Hsin Lin, Daniel Wei & Qingyan Chen (2016) Experimental and numerical study of airflow distribution in an aircraft cabin mock-up with a gasper on, Journal of Building Performance Simulation, 9:5, 555-566, DOI: 10.1080/19401493.2015.1126762

To link to this article: http://dx.doi.org/10.1080/19401493.2015.1126762

Published online: 13 Jan 2016.

Journal of Building Performance Simulation, 2016
Vol. 9, No. 5, 555–566, http://dx.doi.org/10.1080/19401493.2015.1126762

Taylor & Francis
Taylor & Francis Group

Experimental and numerical study of airflow distribution in an aircraft cabin mock-up with a gasper on

Ruoyu You[a], Jun Chen[a], Zhu Shi[a], Wei Liu[a,b], Chao-Hsin Lin[c], Daniel Wei[d] and Qingyan Chen[a,b]*

[a]*School of Mechanical Engineering, Purdue University, West Lafayette, IN 47907, USA;* [b]*Tianjin Key Laboratory of Indoor Air Environmental Quality Control, School of Environmental Science and Engineering, Tianjin University, Tianjin 300072, China;* [c]*Environmental Control Systems, Boeing Commercial Airplanes, Everett, WA 98203, USA;* [d]*Boeing Research & Technology, Beijing 100027, China*

(*Received 5 May 2015; accepted 28 November 2015*)

Overhead gaspers are prevalently installed in aircraft cabins as a personalized ventilation system. The air distribution in cabins with gaspers on is crucial for creating a thermally comfortable and healthy cabin environment. However, very few studies have investigated the suitable turbulence model to simulation air distribution in cabins with gaspers turned on. This study first conducted experimental measurements of airflow distribution in a mock-up of half of a full-scale, one-row, single-aisle aircraft cabin with a gasper on. Particle image velocimetry was used to measure the complex airflow field above a human simulator. This investigation then used the measured data to evaluate the performance of computational fluid dynamics with the re-normalization group (RNG) k–ε model and the shear stress transport (SST) k–ω model. The results showed that the SST k–ω model was more accurate than the RNG k–ε model for predicting the airflow distribution in gasper-induced jet dominant region in an aircraft cabin.

Keywords: jet flow; computational fluid dynamics (CFD); particle image velocimetry (PIV); Reynolds-averaged Navier-Stokes (RANS); enclosed environments

1. Introduction

Every year, over four billion people arrive at and depart from airports around the world (US DOT 2011). According to a long-term forecast by Airports Council International, this number will double by 2025 (ACI 2007). With the rising popularity of air travel increases, the flying public is increasingly paying attention to the cabin environment. The current environment is not necessarily satisfactory, often being either too hot or too cold (Park et al. 2011). Furthermore, cabin air may contain contaminants such as airborne infectious particles (Olsen et al. 2003), ozone (Bhangar et al. 2008), and volatile organic compounds (Guan, Gao, et al. 2014; Guan, Wang, et al. 2014). The air distribution system plays a major role in controlling the thermal comfort and air quality in cabins (Liu, Mazumdar, et al. 2012). Therefore, it is crucial to investigate the air distribution inside aircraft in order to improve the cabin environment.

Currently, commercial airplanes use a mixing air distribution system to control the cabin environment. A mixing ventilation system supplies conditioned and fresh air to the cabin at ceiling level and then exhausts the cabin air through openings in the side walls at lower level. Experimental measurements in a cabin mock-up (Zhang et al. 2009) and airplane (Liu, Wen, et al. 2012) have indicated that the ventilation effectiveness in an aircraft cabin with this type of system is quite low. Because of the mixing of air, passengers frequently complain about thermal comfort (Hinninghofen and Enck 2006) and air quality (Nagda and Hodgson 2001; Spengler and Wilson 2003). Moreover, both experimental and numerical studies have demonstrated that the mixing air distribution increases the risk of infection by airborne diseases (Gupta, Lin, and Chen 2011; Li et al. 2014).

In order to improve the cabin environment, a system of gaspers is typically installed to provide personalized ventilation. Normally, one gasper is situated above the seat of each passenger. The gaspers are adjustable for both supply air velocity and direction, thus allowing passengers to improve their individual thermal comfort. Furthermore, because gaspers provide clean air directly to the passengers, it may be logically assumed that their use reduces exposure to air contaminants in the cabin. Dai et al. (2015) have measured the jet flow in the near-gasper region with a high precision hot-wire anemometer, and then analysed its characteristics such as self-similarity. Shi, Dai, et al. (2015) have validated the SST k–ω model for calculating gasper-induced airflow with the experimental data. Although gaspers are widely used in aircraft cabins, there

*Corresponding author. Email: yanchen@purdue.edu

have been surprisingly few studies of air distribution in cabins with the gaspers turned on.

To investigate the air distribution in a cabin with gaspers on, computational fluid dynamics (CFD) is the most popular because it can provide informative and accurate air distribution results in aircraft cabins. For instance, Yan et al. (2009) used the standard k–ε model to calculate the air distribution in an occupied Boeing 767 mock-up. Zhang et al. (2009) and Gupta, Lin, and Chen (2011) applied a re-normalization group (RNG) k–ε model (Yakhot and Orszag 1986) with a Lagrangian method to predict the airflow field and particle transport in an aircraft cabin. Liu et al. (2013) compared the performance of the RNG k–ε model, large eddy simulation (LES) (Smagorinsky 1963; Deardorff 1970), and detached eddy simulation (Spalart et al. 1997; Shur et al. 1999) in predicting air distribution in a commercial airplane. The review by Liu, Mazumdar, et al. (2012) concluded that the RNG k–ε model was the most robust turbulence model for cabin airflow simulations. Although LES can provide more accurate results, its computing cost is very high (Liu, Mazumdar, et al. 2012). It should be noted that the studies above were designed for investigating the main airflow field rather than gasper-induced airflow. The latter has similar features to a jet with very high gradients of pressure, velocity, and temperature, which make the LES simulation even less affordable. However, Shi, Chen, and Chen (2015) found the shear stress transport (SST) k–ω model to be superior in predicting jet flow. The air distribution in a cabin with gaspers turned on may be dominated by both the main airflow and gasper-induced airflow. Therefore, it is worthwhile to compare the RNG k–ε and SST k–ω models in order to identify a suitable turbulence model for predicting such airflow with a reasonable computing cost.

Experimental methods have typically used hot-wire, hot-sphere, and ultrasonic anemometers, and optical anemometers such as particle image velocimetry (PIV) (Liu, Mazumdar, et al. 2012). For accurate measurements of airflow distribution in a cabin mock-up with a gasper on, however, not all the above-mentioned instruments can be used. Hot-wire and hot-sphere anemometers (HSAs) are unsuitable because their resolutions are generally poor and there are great uncertainties in the results (Liu, Mazumdar, et al. 2012). Ultrasonic anemometers are too bulky for use in a small area (Liu, Mazumdar, et al. 2012) where gasper-induced airflow is dominant. In contrast, PIV determines the air velocity by use of particles injected into the airflow, a technique that provides air velocity vector data with a high spatial resolution (Cao, Liu, Jiang, et al. 2014; Cao, Liu, Pei, et al. 2014). Therefore, PIV seems the most suitable experimental method for obtaining high-quality experimental data of airflow distribution in an aircraft cabin with gaspers on.

This study first conducted experimental measurements of the airflow field in an aircraft cabin mock-up with a gasper on using PIV to obtain high-quality data. The airflow features from the mock-up are similar to those found in actual airliner cabins. The data were then used to evaluate the RNG k–ε and SST k–ω models, which are the most promising models according to the above review. With this effort, it was possible to identify a suitable model for studying airflow distribution in an actual aircraft cabin with gaspers on.

2. Methods

2.1. *Experimental method*

2.1.1. *Experimental setup*

The main objective of this paper was to identify a suitable turbulence model for calculating airflow distribution in an aircraft cabin with gaspers on. The research required very high-quality experimental data to validate the model while the data must contain all the flow characteristics found in actual cabins. Complex cabin mock-ups and real aircraft cabins were not preferable for model evaluation. For instance, Zhang et al. (2009) measured the airflow field in a section of half occupied, twin-aisle cabin mock-up with complex geometry. Liu et al. (2013) further measured the airflow field in the first-class cabin of a functional MD-82 airplane with heated manikins. Since the mock-up and airplane were very complex in geometrical and thermos-fluid boundary conditions, it was impossible to control the boundary conditions. For example, the air supply from the main diffusers was highly non-uniform and three-dimensional; the heat flux from manikins with human shape was also non-uniform; and the pressure difference along the longitudinal direction was not zero that formed a strong longitudinal flow. Thus, the uncertainties in the experimental data would be much greater than the model difference as reported in Zhang et al. (2009) and Liu et al. (2013). Therefore, this study designed such a simplified cabin mock-up that contained all the most important flow mechanism such as inertial force from a gasper, thermal plume from a heat box with uniform heat flux, and a geometry close to an air cabin.

This study built a simplified full-scale mock-up of half of a one-row, single-aisle aircraft cabin with dimensions of 3.5 m in width (x), 0.9 m in depth (y), and 2.2 m in height (z), as shown in Figure 1. The main airflow entered in a downward direction from a linear diffuser on the aisle ceiling, and the exhaust was located on the right-side wall at floor level. The environmental control system supplied air at a velocity of 1.44 m/s. The enclosures were well insulated so that a stable thermal condition was maintained in the cabin mock-up. A gasper was installed on the inclined surface of the ceiling, and it supplied air at a flow rate of 1.2 l/s. The total airflow from the main ventilation system and the gasper was 27.1 l/s. This total airflow was equivalent to an air change rate of 33.5 ACH, which is similar to the air change rate (33.7 ACH) in a published study on droplet transport in an aircraft cabin (Gupta, Lin, and Chen 2011).

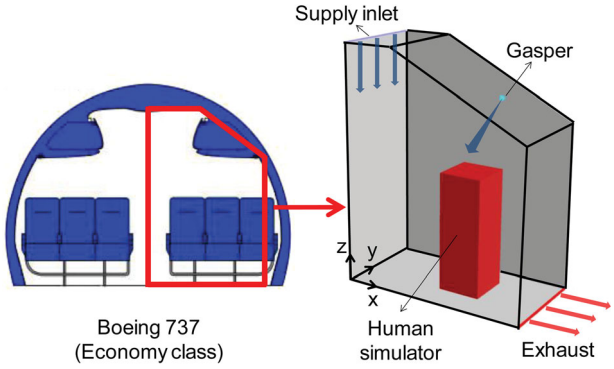

Figure 1. Configuration of the aircraft cabin mock-up (in color online).

A heated human simulator was used to represent a passenger inside the cabin. The sensible heat load of the simulator was controlled at 75 W. Although the cabin mock-up was different from an actual cabin, the experiment was meaningful because the airflow characteristics should have been similar to those in a cabin.

As illustrated in Figure 2(a), the airflow field in the area directly above the human simulator was the most complex, because the main airflow, the gasper-induced airflow, and the thermal plume generated by the human simulator interacted in this region. This investigation used a PIV system (LaVision) to measure the two-dimensional airflow field in an area above the simulator as identified in Figure 2(b). The PIV system consisted of a laser generator and a camera with a resolution of 2048 × 2028 pixels. The laser beam was transmitted to a 1-mm-thick laser sheet by a set of lenses. A fog generator with an aqueous glycol solution was used to generate fine particles with a diameter of 1–2 μm. Particles with a diameter in this range (< 3 μm) are able to follow the flow faithfully (Cao, Liu, Pei, et al. 2014). In addition to the PIV measurement in the critical area, this study also used HSAs to measure the air velocity magnitude and temperature in the locations where the gasper-induced jet had limited impact, as shown in Figure 2(b). This investigation used thermocouples to measure the supply air temperature and all the surface temperatures.

2.1.2. *Experimental procedure*

Before the experiment, the environmental control system for the cabin mock-up was operated for about five hours to achieve a stable air distribution. In the PIV system used in this study, each camera was able to measure a sub-area of 0.16 × 0.16 m^2 with high quality. Since there were two cameras, 12 sub-areas were measured in six independent tests in order to complete the whole measurement area shown in Figure 2(b). Each test captured 800 pairs of images in the sub-area with a time step size of 0.001 s, providing accurate and statistically meaningful information about the air velocity field with a resolution of 128 × 128 data points. Thus, the whole measurement area contained 512 × 384 data points. This investigation also measured the air velocity and temperature in other areas as shown in Figure 2(b) using HSAs. Furthermore, the supply air temperature and all the surface temperatures were measured using thermocouples as listed in Table 1.

The complete experiment was conducted twice on different days. As shown in Figure 3, these two independent

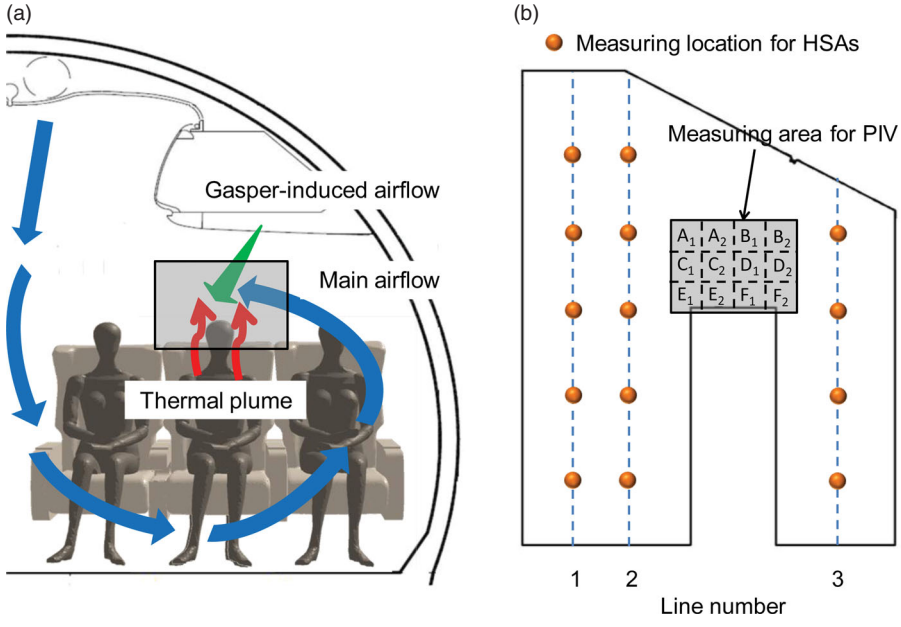

Figure 2. Setup for experimental measurements: (a) critical area where the main airflow, gasper-induced airflow, and thermal plume interacted; (b) measurement area for airflow field by PIV and measurement locations for air velocity and temperature by HSAs (in color online).

Table 1. Measured boundary conditions.

Boundary	Temperature (°C)	Boundary	Temperature (°C)
Front wall ($-y$)	19.7	Rear wall ($+y$)	19.2
Left wall ($-x$)	18.5	Right wall ($+x$)	19.2
Ceiling ($+z$)	19.0	Floor ($-z$)	19.4
Supply air (main)	18.4	Supply air (gasper)	17.9
Human simulator	24.5		

measurements of air velocity and temperature by the HSAs matched each other closely. This result indicates that the experiment was repeatable.

2.2. *Numerical method*

2.2.1. *Geometry of the gasper*

Figure 4(a) shows a photograph of the gasper that was used in this study. The diameters of the upper and lower round sections were 35 and 17.7 mm, respectively. The air supply inlet was annular in shape and was located inside the gasper. The diameter of the annular inlet was 12.6 mm, and the total inlet area was 33.4 mm^2. This study created a detailed geometry of the gasper on the basis of measured dimensions of the actual gasper, as shown in Figure 4(b). The detailed geometry is essential for fully capturing the characteristics of the gasper-induced airflow.

2.2.2. *Turbulence models*

This investigation evaluated the RNG k–ε and SST k–ω models for predicting airflow distribution in aircraft cabins with gasper on. The RNG k–ε model is the most popular and robust for simulations of cabin airflow (Liu, Mazumdar, et al. 2012), while the SST k–ω model is superior for a jet flow (Shi, Chen, and Chen 2015). These two models are two-equation Reynolds-averaged Navier-Stokes (RANS) eddy-viscosity models. Boussinesq eddy-viscosity hypothesis was used to link the turbulence Reynolds stresses to eddy-viscosity. The models then introduce two more transport equations for turbulence quantities to close the equation system.

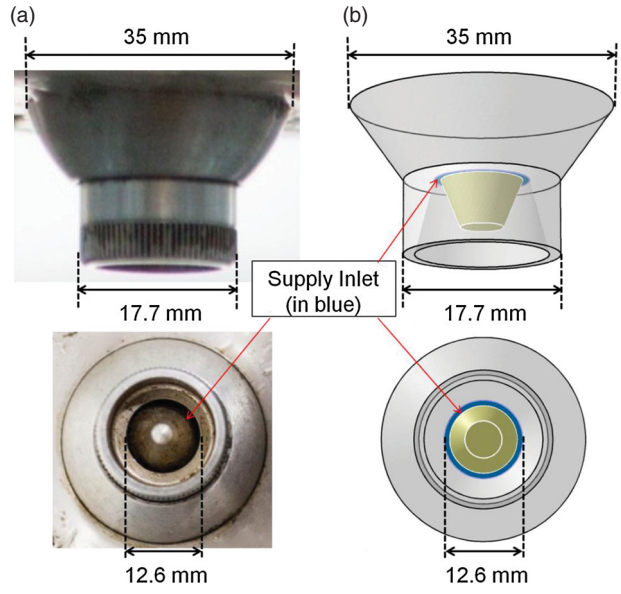

Figure 4. Gasper used in this study: (a) photograph and (b) computer model (in color online).

The k–ε models solve two transport equations for turbulent kinetic energy (k), and turbulence dissipation rate (ε). Launder and Spalding (1974) developed the standard k–ε model based on experimental data of free shear turbulent flows. Therefore, standard k–ε model is appropriate for fully turbulent jets and mixing layers. The RNG k–ε model (Yakhot and Orszag 1986; Choudhury 1993) was developed to account for the effects of smaller scales of motion based on the mathematical technique called RNG methods. For indoor environments, RNG k–ε model is found to be the most robust and accurate turbulence model (Chen 1995; Zhang et al. 2007; Wang and Chen 2009). In addition, since the RNG k–ε model was developed for fully turbulent flows, wall functions were required for near wall region when simulating wall-bounded flow.

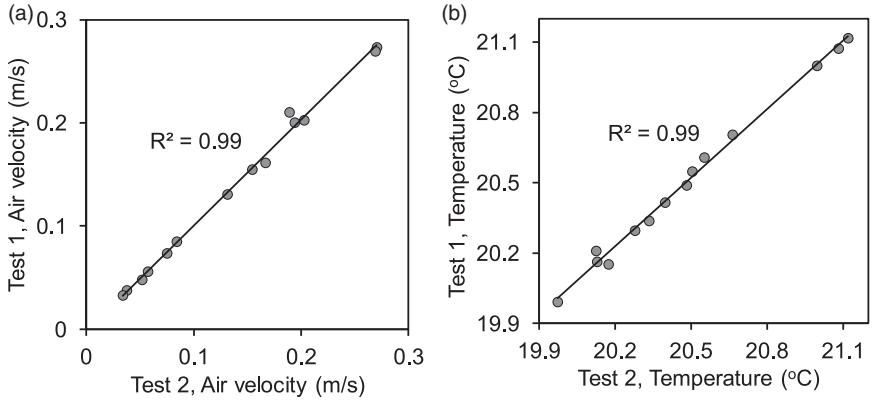

Figure 3. Comparison of two independent measurements of (a) air velocity and (b) temperature using HSAs.

In the k–ω models, a transport equation of specific turbulence dissipation rate (ω) is used instead of ε, where ω is the ratio of ε to k. The standard k–ω model developed by Wilcox (1988) is resolved in the near wall region. Compared with the k–ε models, it is thus superior in predicting equilibrium adverse pressure flows (Wilcox 1988; Huang, Bradshaw, and Coakley 1992). However, the mean velocity of free shear flows and wake region predicted by standard k–ω model is sensitive to free stream turbulence (Menter 1994). To take advantage of both models, the SST k–ω model (Menter 1994) was developed as an integrated model of the standard k–ε model and standard k–ω model. The SST k–ω model utilizes the standard k–ω model in the near wall region, and activates a transformed standard k–ε model in the free shear region. Blending functions are employed to gradually switch on and off the two models. Therefore, the SST k–ω model is suitable for both free shear region and near wall region with equilibrium adverse pressure flows.

Note that the air distribution in the occupied zone of a cabin with gaspers turned on may be dominated by both the main airflow and gasper-induced jet flow. As discussed above, the RNG k–ε model is the most popular and robust for simulations of cabin main airflow, and the SST k–ω model is suitable for both free shear jet and boundary layer. Therefore, this study chose these two models to evaluate their performances in predicting the air distribution in the occupied zone of a cabin with gaspers on.

2.2.3. *Numerical methods*

This study adopted the Boussinesq approximation to simulate the buoyancy effect. The SIMPLE algorithm was employed to couple the pressure and velocity. This investigation used the first-order scheme for pressure discretization and the second-order upwind scheme for discretizing all the other variables. Such discretization strategy has been proven effective by many previous studies (e.g. Zhang et al. 2007; Wang and Chen 2009; Liu et al. 2013). The Fluent's enhanced wall treatment (ANSYS 2010) was applied in the simulation with the RNG k–ε model. The enhanced wall treatment implements hybrid wall functions, which is suitable for varying $y+$. For the SST k–ω model, the near wall cells should be in the viscous layer region where the $y+$ should preferably less than 5. When the sum of the normalized residuals for all the cells was smaller than 10^{-4} for velocity and turbulence quantities and 10^{-6} for energy, the solutions were considered to be converged.

For the aircraft cabin mock-up, this study generated a hybrid mesh that consisted of hexahedral, prismatic, pyramidal, and tetrahedral cells, as shown in Figure 5. Unstructured grids (tetrahedral and pyramidal) were used in the region near the gasper (section 1) to depict its complex geometry, while structured grids (hexahedral and prism) were used in other regions (sections 2 and 3) to reduce the total grid number. Three grid resolutions, 0.7, 1.58, and 3.07 million, were tested for CFD grid independence. The resolution of 1.58 million was sufficiently fine to capture the turbulent flow in the chamber. Under this grid resolution, the mesh size in section 1 ranged from 0.3 to 1 mm, while in other sections it ranged from 1 to 16 mm. The corresponding averaged $y+$ for the gasper surface was around 6. Since the SST k–ω model resolves the near wall region instead of using a wall function, it is worthwhile to verify that the minimum size of 0.3 mm to be sufficient. Therefore, we compared our simulated jet centreline velocity from a gasper by the SST k–ω model with the measured data from Dai et al. (2015). The jet flow in the near-gasper region was measured by a high precision hot-wire anemometer. In Figure 6, U_m is the mean centreline velocity, U_{peak} is the maximum mean centreline velocity, s is the axial distance from the gasper, s_{peak} is distance corresponding to U_{peak}, and D is the diameter of the gasper annular inlet (12.6 mm). The results shown in Figure 6 confirmed that the grid size used in this study was sufficient. The volume of the near-gasper region was only 0.0006% of the total volume of the cabin. Nevertheless, this region contained 28% of the total number of cells. The complex geometry of the gasper resulted in a considerable increase in the total cell number.

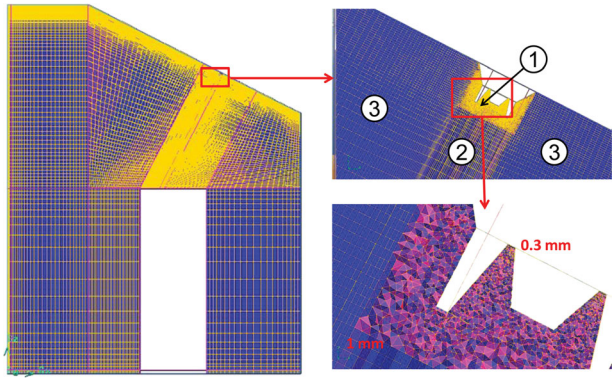

Figure 5. Hybrid hexahedral, prismatic, and tetrahedral grids for the aircraft cabin mock-up (in color online).

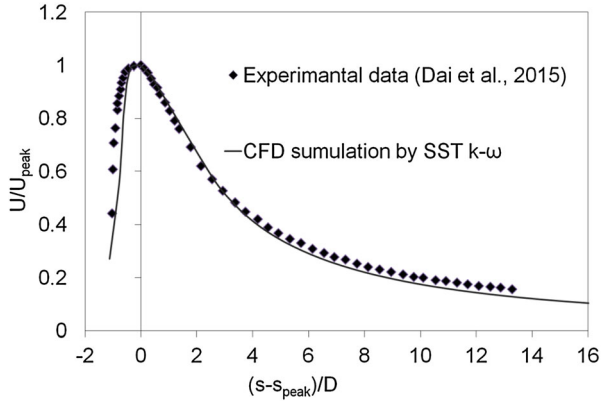

Figure 6. Comparison of the predicted non-dimensional mean centreline velocity profile with the measured data from Dai et al. (2015).

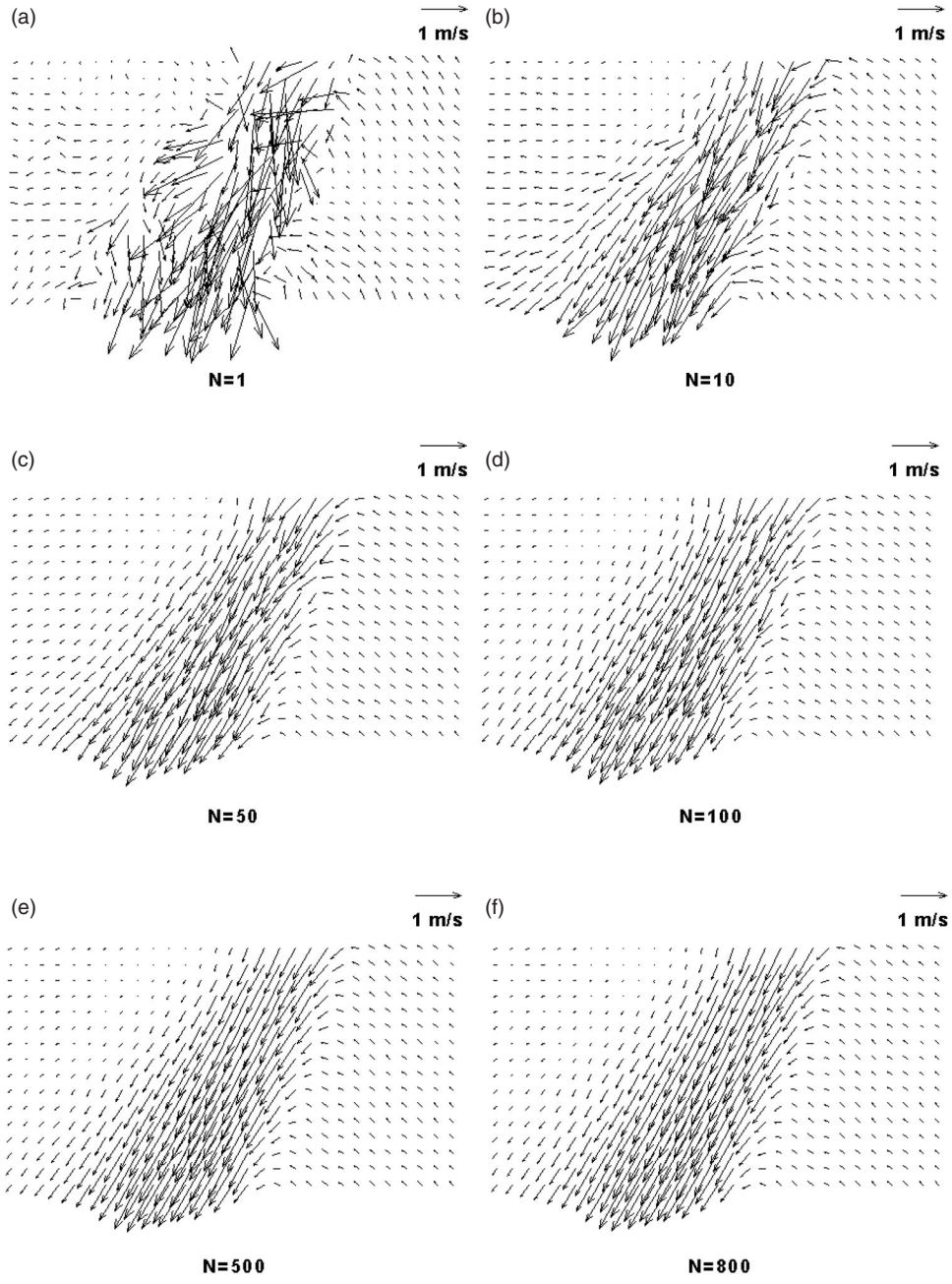

Figure 7. The time-averaged airflow field in section B from (a) one image, (b) 10 images, (c) 50 images, (d) 100 images, (e) 500 images, and (f) 800 images.

3. Results

3.1. Experimental results

This investigation used PIV to measure the airflow field in the critical area in the cabin mock-up. This study first conducted a sensitivity analysis of the number of images used. As mentioned above, 12 sub-areas were measured in six independent tests to complete the whole measurement area shown in Figure 2(b). It should be noted that because the airflow fields in the six sub-sections were measured at different times, they could not be combined together at a single time point. Therefore, only one section was used for the sensitivity analysis. Figure 7 compares the time-averaged airflow field for section B from 1, 10, 50, 100, 500, and 800 images, respectively. The single-image result shown in Figure 7(a) was not smooth. The time-averaged airflow field became smoother with as the number of images increased. A strong jet profile was observed when the number of images reached 50. When the number of images reached 800, a smooth and converged vector field was obtained.

Figure 8 shows the time-averaged airflow field obtained by averaging 800 images for each sub-area to

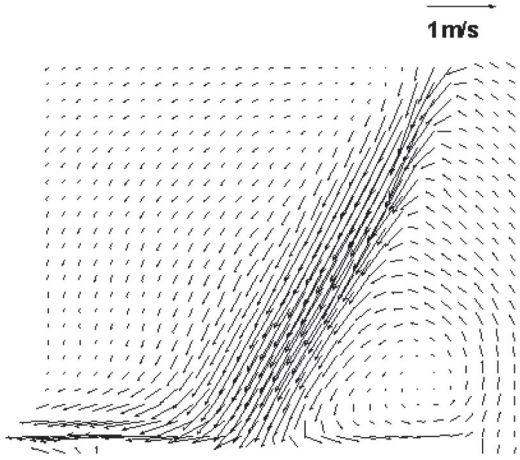

Figure 8. The time-averaged airflow field in the measurement area obtained from 800 measured images.

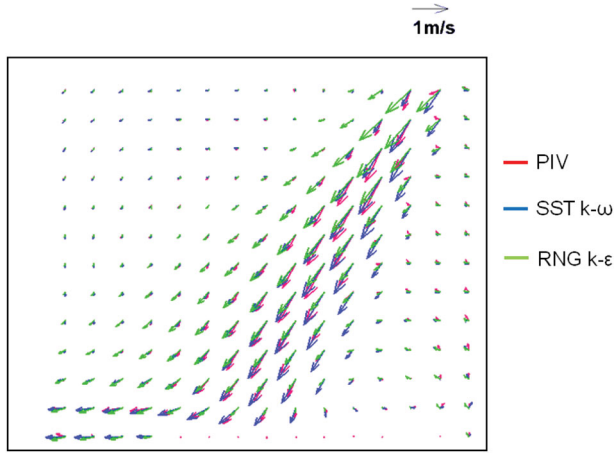

Figure 9. Comparison of the predicted airflow field and experimental data in the critical area (in color online).

form the entire region as shown in Figure 2(b). Although the sub-areas were measured in six different tests, the transitions between sub-areas were smooth. A strong jet structure was observed from the upper right to the lower left part of the measurement area, and the jet decayed as it developed. The direction of the main flow in the lower right corner of the cabin is upward. A clear vortex structure formed in the lower right part of the area. This vortex may have resulted from the interaction between the gasper-induced jet, the thermal plume generated by the human simulator, and the main flow in the cabin. The data obtained from the experiment will be used to evaluate the chosen CFD models.

3.2. *Model evaluation*

This study first evaluated ability of the RNG k–ε and SST k–ω models to predict airflow distribution in the critical area (as shown in Figure 2(b)) by comparing their results with the measured data obtained by PIV. Figure 9 compares the predicted two-dimensional airflow field with the experimental data in the critical area. To make the comparison more easily observable, the resolutions of the experimental data were reduced from 512 × 384 to 15 × 14. The corresponding data points predicted by the two models were used for the comparison. Both models correctly predicted a strong jet traveling from the upper right-hand side to the lower left-hand side. Furthermore, both models were able to capture the small circulation pattern on the lower right-hand side that was caused by the interaction between the gasper-induced flow and the thermal plume generated by the human simulator. However, the RNG k–ε model obviously under-predicted the velocity magnitude of the gasper-induced flow in the critical area.

To further analyse the numerical results, Figure 10 compares the predicted and measured velocity profiles in the horizontal (x) and vertical (z) directions at five lines in the critical area. It should be noted that both the predicted and measured data in the figure contained the air velocity in only the x and z directions. In the horizontal direction, the velocity profiles predicted by the SST k–ω model were in very good agreement with the experimental data, as shown in Figure 10(a). The SST k–ω model correctly captured the peak velocity at each line. However, the agreement between the results from the RNG k–ε model and the data measured by PIV was unsatisfactory, because the RNG k–ε model failed to capture the peaks. In the vertical direction, the velocity profiles predicted by the SST k–ω model again agreed very well with the experimental data, as shown in Figure 10(b). However, as in the horizontal direction, the RNG k–ε model failed to accurately predict the velocity profile in the vertical direction, especially at lines 3, 4, and 5. The measured airflow field indicates that the gasper-induced jet dominated in the critical area. Since the SST k–ω model was superior in predicting a jet flow (Shi, Chen, and Chen 2015), it tended to be more accurate than the RNG k–ε model in predicting the air velocity distribution in the critical area of the aircraft cabin mock-up.

To quantitatively compare the accuracy of the models, the normalized root mean square errors (NRMSE) between the predicted and measured data were calculated by:

$$\mathrm{NRMSE} = \frac{\sqrt{\left(\sum_{i=1}^{n}\left(\phi_{\mathrm{exp},i} - \phi_{\mathrm{model},i}\right)^2\right)/n}}{\phi_{\mathrm{exp,max}} - \phi_{\mathrm{exp,min}}}, \qquad (1)$$

where $\phi_{\mathrm{exp},i}$ is a data point from the experimental data, $\phi_{\mathrm{model},i}$ is the corresponding data point from the modelling results, and $\phi_{\mathrm{exp,max}}$ and $\phi_{\mathrm{exp,min}}$ are the maximum and minimum value of experimental data, respectively. Table 2 lists the calculated NRMSEs between the predicted and measured horizontal and vertical velocity in the critical area. As shown in Table 2, the NRMSEs for the SST k–ω model were significantly lower than the RNG k–ε model. Thus, the SST k–ω model is more appropriate for predicting the air distribution in the occupied zone of a cabin.

This investigation also compared the predicted turbulence feature by the SST k–ω and RNG k–ε models with

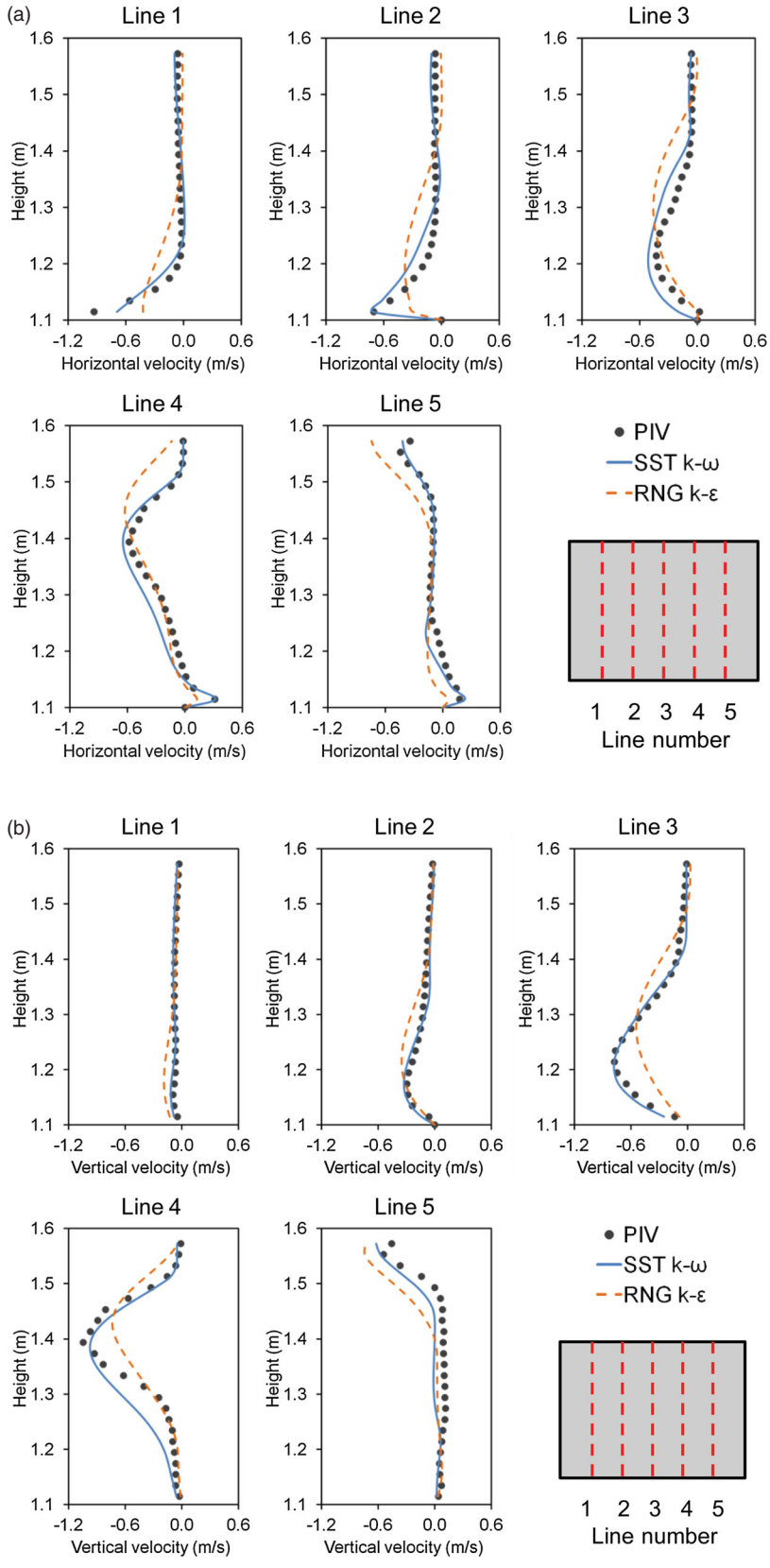

Figure 10. Comparison of the predicted and measured velocity profiles in (a) the horizontal and (b) the vertical direction in the critical area (in color online).

Table 2. NRMSE between the predicted air velocity and the data measured by PIV for the turbulence models.

	NRMSE	
Compared parameter	SST k–ω model	RNG k–ε model
Horizontal velocity by PIV	0.06	0.13
Vertical velocity by PIV	0.08	0.12

the measured data. Since the measured data were only two-dimensional, the turbulence features were defined as $\sqrt{\overline{(u'_x)^2} + \overline{(u'_z)^2}}$, where u'_x and u'_z represent the turbulent fluctuating velocity in the x and z directions, respectively. Both the RNG k–ε and SST k–ω models assume the flow to be isotropic, and thus the predicted turbulence feature was calculated by:

$$\sqrt{\overline{(u'_x)^2} + \overline{(u'_z)^2}} = 2\sqrt{\frac{k}{3}}, \tag{2}$$

where k is the turbulence kinetic energy determined by CFD. Figure 11 compares the predicted and measured turbulent feature profiles at the five lines in the critical area. It can be seen that the performance of the SST k–ω model was better than that of the RNG k–ε model at lines 2 and 3 and similar to that of the RNG k–ε model at line 5, but it was worse at lines 1 and 4. Generally speaking, the overall accuracy of the RNG k–ε and SST k–ω models in predicting the turbulence feature was similar in the critical area. The discrepancies between predicted and measured data may be attributable to the isotropic flow assumption of the two models.

Figure 12 compares the predicted velocity profiles and the data measured by HSAs in the regions of the cabin where the gasper-induced airflow had limited impact on the airflow pattern. The error bars represented the standard uncertainty of the measured data with a confidence level of 68.3%. At lines 1 and 2 as shown in Figure 2(b), both the RNG k–ε and SST k–ω models were able to predict the air velocities within the error bars. The lower region at line 1 was directly affected by the main supply airflow, so that the air velocities were relatively large. The peak velocity at the height of 1.1 m at line 2 occurred because of the jet from the gasper. Both models were able to capture this phenomenon. At line 3, however, the results predicted by the RNG k–ε model were slightly better than those predicted by the SST k–ω model. Figure 13 further compares the predicted temperature profiles and the data measured by the HSAs in the regions of the cabin where the gasper-induced airflow had limited impact. Both the experimental data and the simulation results show a rather uniform temperature distribution with a temperature difference of less than 2°C in the cabin mock-up. Both the measured and calculated results exhibit slight positive vertical temperature

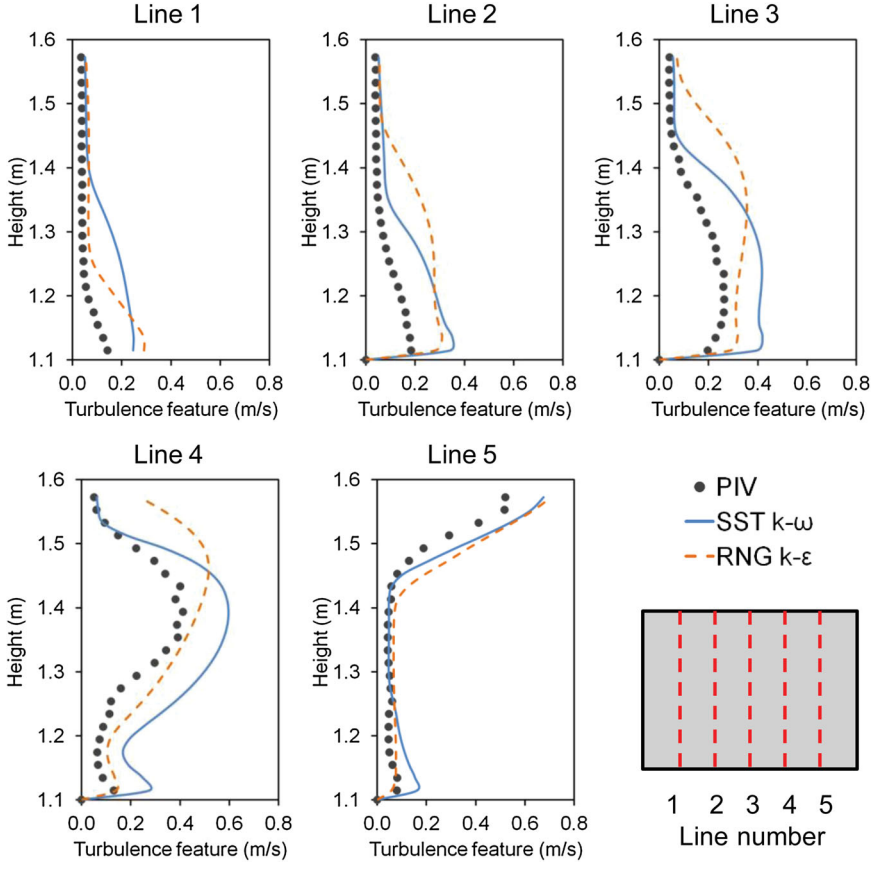

Figure 11. Comparison of the predicted and measured turbulent feature $\left(\sqrt{\overline{(u'_x)^2} + \overline{(u'_z)^2}}\right)$ in the critical area (in color online).

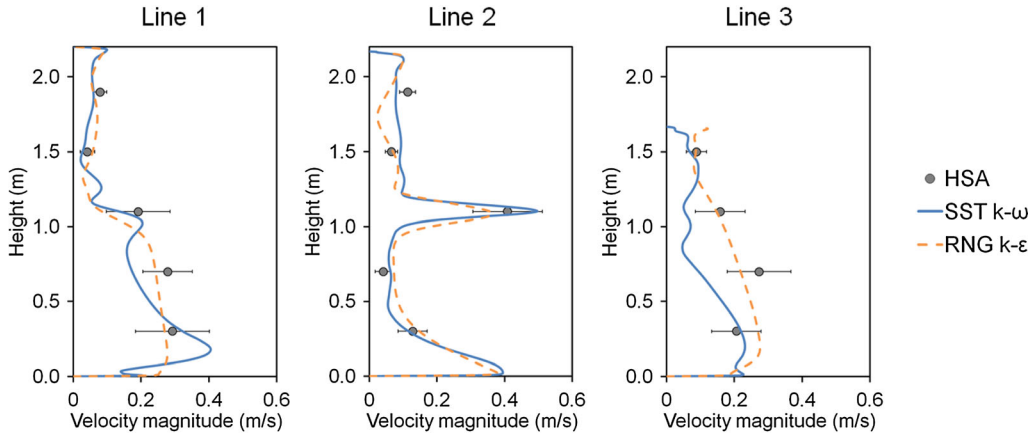

Figure 12. Comparison of the predicted velocity profiles and the data measured by HSAs in the cabin.

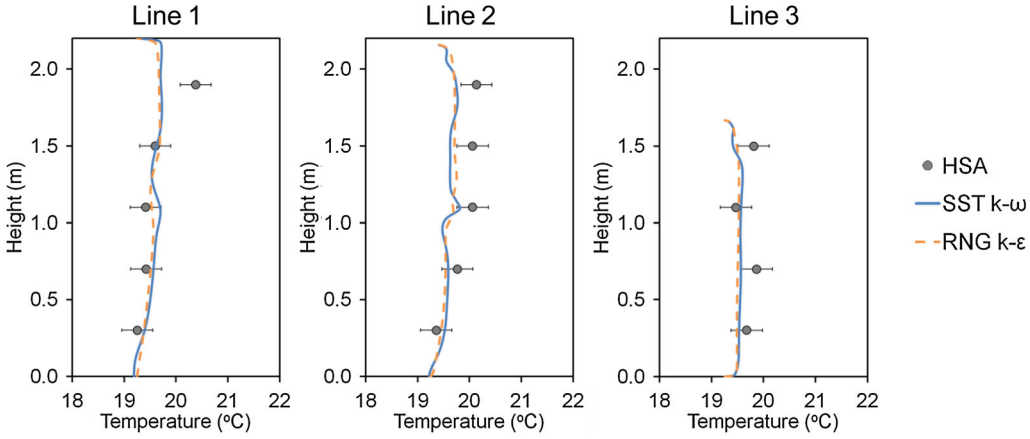

Figure 13. Comparison of the predicted temperature profiles and the data measured by HSAs in cabin regions where the gasper-induced airflow had limited impact (in color online).

Table 3. NRMSE between the predicted results and the data measured by HSAs for the turbulence models.

	NRMSE	
Compared parameter	SST k–ω model	RNG k–ε model
Velocity magnitude by HSA	0.19	0.12
Temperature by HSA	0.27	0.27

gradients at all the lines. Both models accurately predicted the temperature profiles at these lines when compared with the experimental data. Generally speaking, in the regions where the gasper-induced jet had limited impact on the airflow pattern, the RNG k–ε model predicted a slightly better air velocity and temperature distribution in the cabin mock-up than did the SST k–ω model, which was supported by the calculated NRMSEs shown in Table 3.

4. Discussion

4.1. Limitations

This investigation built a full-scale mock-up of half of a one-row, single-aisle aircraft cabin for measuring airflow distribution above the human simulator of the cabin mock-up with a gasper on. Although this experimental setup was quite different from an actual cabin, it contained the main flow features in a cabin, including the circulated main airflow, gasper-induced airflow, and the thermal plume generated by the human simulator. Therefore, because the aim was to provide reliable experimental data for identifying a suitable turbulence model, the experiment was meaningful. The SST k–ω model has been thus identified, and it can be used in the future to calculate the airflow, temperature, and contaminant concentration distributions in actual aircraft. Such future investigations would provide a greater understanding of the influence of gasper-induced airflow on thermal comfort and cabin air quality.

Furthermore, the PIV measurements in this study were only two-dimensional. The turbulence kinetic energy could not be obtained with the two components of measured turbulence fluctuating velocities. This problem could be solved by using three-dimensional PIV measurements, which also deserves further study. In addition, other factors such as boundary conditions may also affect the accuracy of the models in predicting turbulence quantities.

4.2. Characteristics of the gasper-induced airflow in the aircraft cabin mock-up

The comparison above has identified the SST k–ω model as the most suitable one for predicting airflow distribution in an aircraft cabin. This section analyses the numerical results from the SST k–ω model in detail in order to characterize this airflow. For gasper-induced flow, Dai et al. (2015) and Shi, Dai, et al. (2015) showed that the annular jet flow merged together and further developed as would a round jet.

To explore the similarity between a gasper-induced jet in an aircraft cabin and a round jet, this study compared the mean centreline velocity (U_m) decay as a function of axial distance (s) for the two jet types, as shown in Figure 14. The mean centreline velocity decay of the gasper-induced jet was obtained from the CFD simulation, while that of a round jet was derived on the basis of jet theory. For a round jet in the fully developed region, U_m is proportional to the inverse of the axial distance from the jet inlet, which can be expressed as (Pope 2000; Hussein, Capp, and George 1994):

$$\frac{U_m}{U_{m,0}} = \frac{B}{(s - s_0)/d}, \tag{3}$$

where B is an empirical constant, d is the diameter of the round jet, $U_{m,0}$ is the exit velocity of the round jet, s is the axial distance from the round inlet, and s_0 is the position of the virtual jet origin. For gasper-induced flow, the variable s was defined as the axial distance from the lower bound of the gasper. Derived from Equation (11), U_m as a function of s could be expressed as:

$$U_m = \frac{B^*}{s - s_0}, \tag{4}$$

where B^* is an empirical constant. By means of a least-squares regression analysis, it was found that a B^* of 0.83 with an s_0 of 0 would fit the CFD simulation data best in the axial distance range of 0.09 to 0.58 m (zone ② in Figure 14), with an R^2 of 0.99. Therefore, it was possible to regard the gasper-induced jet as a fully developed round jet in zone ②. When the distance was less than 0.09 m (zone ① in Figure 14), the gasper-induced jet was quite complex as discussed in Dai et al. (2015) and Shi, Dai, et al. (2015), thus unlike a round jet. When the distance was greater than 0.58 m (zone ③ in Figure 14), the velocity decay profile of the gasper-induced jet differed significantly from that of a round jet. This result indicates that, in zone ③, the gasper-induced jet was affected by both the main airflow in the cabin and the thermal plume generated by the human simulator. The analysis in this section provides a clearer understanding of gasper-induced airflow in the aircraft cabin mock-up.

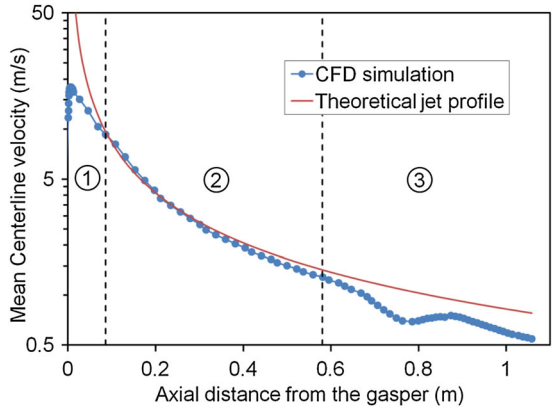

Figure 14. Gasper-induced jet mean centreline velocity decay as a function of axial distance from the gasper (in color online).

5. Conclusions

This investigation measured the airflow field in an aircraft cabin mock-up with a gasper on and then evaluated two turbulence models by comparing their results with experimental data. Within the scope of this research, the following conclusions can be drawn:

(1) The PIV technique can obtain high-resolution experimental data on airflow distribution of the critical area in an aircraft cabin mock-up.
(2) The SST k–ω model is more accurate than the RNG k–ε model for predicting the airflow distribution in gasper-induced flow dominant region in an aircraft cabin.
(3) In regions where gasper-induced airflow has limited impact on the airflow pattern, the RNG k–ε model provides slightly better airflow predictions than does the SST k–ω model.

Disclosure Statement

No potential conflict of interest was reported by the authors.

Funding

The research presented in this paper was partially supported by the National Basic Research Program of China (the 973 Program) [grant number 2012CB720100].

ORCID

Qingyan Chen http://orcid.org/0000-0002-3204-9488

References

ACI (Airports Council International). 2007. "The Global Airport Community." www.airports.org/aci/aci/file/AnnualReport/ACIAnnualReport2006FINAL.pdf.

ANSYS. 2010. "Fluent 12.1 Documentation." Lebanon, NH: Fluent Inc.

Bhangar, S., S. C. Cowlin, B. C. Singer, R. G. Sextro, and W. W. Nazaroff. 2008. "Ozone Levels in Passenger Cabins of

Commercial Aircraft on North American and Transoceanic Routes." *Environmental Science and Technology* 42: 3938–3943.

Cao, X., J. Liu, N. Jiang, and Q. Chen. 2014. "Particle Image Velocimetry Measurement of Indoor Airflow Field: A Review of the Technologies and Applications." *Energy and Buildings* 69: 367–380.

Cao, X., J. Liu, J. Pei, Y. Zhang, J. Li, and X. Zhu. 2014. "2D-PIV Measurement of Aircraft Cabin Air Distribution with a High Spatial Resolution." *Building and Environment* 82: 9–19.

Chen, Q. 1995. "Comparison of Different k–ε Models for Indoor Air Flow Computations." *Numerical Heat Transfer, Part B* 28: 353–369.

Choudhury, D. 1993. "Introduction to the Renormalization Group Method and Turbulence Modeling." Canonsburg, Fluent Inc. Technical Memorandum TM-107.

Dai, S., H. Sun, W. Liu, Y. Guo, N. Jiang, and J. Liu. 2015. "Experimental Study on Characteristics of the Jet Flow from an Aircraft Gasper." *Building and Environment* 93: 278–284.

Deardorff, J. W. 1970. "A Numerical Study of Three-dimensional Turbulent Channel Flow at Large Reynolds Numbers." *Journal of Fluid Mechanics* 42: 453–480.

Guan, J., K. Gao, C. Wang, X. Yang, C-H. Lin, C. Lu, and P. Gao. 2014. "Measurements of Volatile Organic Compounds in Aircraft Cabins. Part I: Methodology and Detected VOC Species in 107 Commercial Flights." *Building and Environment* 72: 154–161.

Guan, J., C. Wang, K. Gao, X. Yang, C-H. Lin, and C. Lu. 2014. "Measurements of Volatile Organic Compounds in Aircraft cabins. Part II: Target List, Concentration Levels and Possible Influencing Factors." *Building and Environment* 75: 170–175.

Gupta, J. K., C-H. Lin, and Q. Chen. 2011. "Transport of Expiratory Droplets in an Aircraft Cabin." *Indoor Air* 21: 3–11.

Hinninghofen, H., and P. Enck. 2006. "Passenger Well-being in Airplanes." *Autonomic Neuroscience* 129: 80–85.

Huang, P. G., P. Bradshaw, and T. J. Coakley. 1992. "Assessment of Closure Coefficients for Compressible-flow Turbulence Models." NASA TM-103882.

Hussein, H. J., S. P. Capp, and W. K. George. 1994. "Velocity Measurements in a High-reynolds-number, Momentum-conserving, Axisymmetric, Turbulent Jet." *Journal of Fluid Mechanics* 258: 31–75.

Launder, B. E., and D. B. Spalding. 1974. "The Numerical Computation of Turbulent Flows." *Computer Methods in Applied Mechanics and Energy* 3: 269–289.

Li, F., J. Liu, J. Pei, C-H. Lin, and Q. Chen. 2014. "Experimental Study of Gaseous and Particulate Contaminants Distribution in an Aircraft Cabin." *Atmospheric Environment* 85: 223–233.

Liu, W., S. Mazumdar, Z. Zhang, S. B. Poussou, J. Liu, C-H. Lin, and Q. Chen. 2012. "State-of-the-art Methods for Studying Air Distributions in Commercial Airliner Cabins." *Building and Environment* 47: 5–12.

Liu, W., J. Wen, J. Chao, W. Yin, C. Shen, D. Lai, C-H. Lin, J. Liu, H. Sun, and Q. Chen. 2012. "Accurate and High-resolution Boundary Conditions and Flow Fields in the First-class Cabin of an MD-82 Commercial Airliner." *Atmospheric Environment* 56: 33–44.

Liu, W., J. Wen, C-H. Lin, J. Liu, Z. Long, and Q. Chen. 2013. "Evaluation of Various Categories of Turbulence Models for Predicting Air Distribution in an Airliner Cabin." *Building and Environment* 65: 118–131.

Menter, F. R. 1994. "Two-equation Eddy-viscosity Turbulence Models for Engineering Applications." *AIAA Journal* 32: 1598–1605.

Nagda, N. L., and M. Hodgson. 2001. "Low Relative Humidity and Aircraft Cabin Air Quality." *Indoor Air* 11: 200–214.

Olsen, S. J., H. Chang, T. Y. Cheung, A. F. Tang, T. L. Fisk, S. P. Ooi, H. Kuo, et al. 2003. "Transmission of the Severe Acute Respiratory Syndrome on Aircraft." *The New England Journal of Medicine* 349: 2416–2422.

Park, S., R. T. Hellwig, G. Grun, and A. Holm. 2011. "Local and Overall Thermal Comfort in an Aircraft Cabin and Their Interrelations." *Building and Environment* 46: 1056–1064.

Pope, S. B. 2000. *Turbulent Flows*. Cambridge: Cambridge university press.

Shi, Z., J. Chen, and Q. Chen. 2015. "On the Turbulence models and Turbulent Schmidt Number in Simulating Stratified Flows." *Accepted by Journal of Building Performance Simulation*. doi:10.1080/19401493.2015.1004109.

Shi, Z., S. Dai, J. Chen, and Q. Chen. 2015. "Numerical Study of Gasper-induced Jet Flow with Detailed Gasper Geometry." Proceedings of the 9th International Symposium on Heating, Ventilating and Air-Conditioning (ISHVAC) and the 3rd International Conference on Building Energy and Environment (COBEE), Tianjin, China. Paper No. T6-573, 9 pp.

Shur, M., P. R. Spalart, M. Strelets, and A. Travin. 1999. "Detached-eddy Simulation of an Airfoil at High Angle of Attack." In 4th International Symposium on Engineering Turbulence Modeling and Experiments, Corsica, France, 9 May.

Smagorinsky, J. 1963. "General Circulation Experiments with the Primitive Equations I: The Basic Experiment." *Monthly Weather Review* 91: 99–164.

Spalart, P. R., W. H. Jou, M. Stretlets, and S. R. Allmaras. 1997. "Comments on the Feasibility of LES for Wings and on the Hybrid RANS/LES Approach." Proceedings of the First AFOSR International Conference on DNS/LES.

Spengler, J., and D. Wilson. 2003. "Air Quality in Aircraft." *Proceedings of the Institution of Mechanical Engineers, Part E: Journal of Process Mechanical Engineering* 217: 323–336.

US DOT (United States Department of Transportation). 2011. "Traffic Data for U.S Airlines and Foreign Airlines U.S. Flights: Total Passengers up from 2009, Still below 2008." Washington, DC.

Wang, M., and Q. Chen. 2009. "Assessment of Various Turbulence Models for Transitional Flows in an Enclosed Environment (RP-1271)." *HVAC&R Research* 15: 1099–1119.

Wilcox, D. C. 1988. "Reassessment of the Scale-determining Equation for Advanced Turbulence Models." *AIAA Journal* 26: 1299–1310.

Yakhot, V., and S. A. Orszag. 1986. "Renormalization Group Analysis of Turbulence." *Journal of Scientific Computing* 1: 3–51.

Yan, W., Y. Zhang, Y. Sun, and D. Li. 2009. "Experimental and CFD Study of Unsteady Airborne Pollutant Transport within an Aircraft Cabin Mock-up." *Building and Environment* 44: 34–43.

Zhang, Z., X. Chen, S. Mazumdar, T. Zhang, and Q. Chen. 2009. "Experimental and Numerical Investigation of Airflow and Contaminant Transport in an airliner Cabin Mockup." *Building and Environment* 44: 85–94.

Zhang, Z., W. Zhang, Z. Zhai, and Q. Chen. 2007. "Evaluation of Various Turbulence Models in Predicting Airflow and Turbulence in Enclosed Environments by CFD: Part-2: Comparison with Experimental Data from Literature." *HVAC&R Research* 13: 871–886.